Water Research 163 (2019) 114846

Contents lists available at ScienceDirect

Water Research

journal homepage: www.elsevier.com/locate/watres

Reactivity of chromophoric dissolved organic matter (CDOM) to sulfate radicals: Reaction kinetics and structural transformation

Suona Zhang [a], Valentin Rouge [a], Leonardo Gutierrez [b, c], Jean-Philippe Croue [a, c, *]

[a] Curtin Water Quality Research Centre, Department of Chemistry, Curtin University, Australia
[b] Facultad del Mar y Medio Ambiente, Universidad del Pacifico, Ecuador
[c] Institut de Chimie des Milieux et des Materiaux IC2MP UMR 7285 CNRS, Universite de Poitiers, France

ARTICLE INFO

Article history:
Received 8 April 2019
Received in revised form
3 July 2019
Accepted 6 July 2019
Available online 7 July 2019

Keywords:
Sulfate radical
CDOM
Reaction kinetics
Structural transformation
Carbon removal

ABSTRACT

Sulfate radical ($SO_4^{\bullet-}$) has been extensively studied as a promising alternative in advanced oxidation processes (AOPs) for water treatment. However, little is known about its reactivity to the ubiquitous dissolved organic matter (DOM) in water bodies. $SO_4^{\bullet-}$ would selectively react with electron rich moieties in DOM, known as chromophoric DOM (CDOM), due to its light absorbing property. In this study, the reactivity and typical structural transformation of CDOM with $SO_4^{\bullet-}$ was investigated. Four well characterized hydrophobic DOM fractions extracted from different surface water sources were selected as model CDOM. $SO_4^{\bullet-}$ was produced through the activation of peroxymonosulfate (PMS) by Co(II) ions at pH 8 in borate buffer. The reactivity of CDOM was studied based on the decrease in its ultraviolet absorbance at 254 nm (UVA_{254}) as a function of time. The reactivity of CDOM changed with time where fast and slow reacting CDOMs (i.e., $CDOM_{fast}$ and $CDOM_{slow}$) were clearly distinguished. A second-order rate constant of $CDOM_{fast}$ with $SO_4^{\bullet-}$ was calculated by plotting UVA_{254} decrease versus PMS exposure; where a R_{ct} value (i.e., ratio of sulfate radical exposure to PMS exposure) was calculated using pCBA as a probe compound. The transformation of CDOM was studied through the analysis of the changes in UVA_{254}, electron donating capacity, fluorescence intensity, and total organic carbon. A transformation pathway leading to a significant carbon removal was proposed. This new knowledge on the kinetics and transformation of CDOM would ultimately assist in the development and operation of $SO_4^{\bullet-}$-based water treatment processes.

1. Introduction

Sulfate radical ($SO_4^{\bullet-}$)-based advanced oxidation processes (AOPs) have gained increasing interest in water treatment at both fundamental and applied levels (Siegrist et al., 2011; Wacławek et al., 2017). Due to its comparable or even stronger oxidizing capabilities than $^{\bullet}OH$, $SO_4^{\bullet-}$ is also capable of degrading a broad spectrum of trace organic contaminants (TOrCs) (e.g., pharmaceuticals, personal care products, and industrial chemicals) which are constantly detected in water bodies (Ghauch et al., 2017; Lutze et al., 2015a). A strong oxidation capacity, together with a high selectivity (i.e., lower scavenging of background organics) (Lutze et al., 2015a), multiple means of radical generation (Wang et al., 2014), and a favored storage/transport of stable solid precursors, make $SO_4^{\bullet-}$ a promising alternative for contaminants removal.

Previous studies focusing on the removal of TOrCs by $SO_4^{\bullet-}$ have provided key mechanistic and kinetic insights (Yang et al. 2017, 2019; Nihemaiti et al., 2018). However, little is known about the $SO_4^{\bullet-}$-induced reactivity and transformation of dissolved organic matter (i.e., DOM, a highly heterogeneous mixture of organic molecules ubiquitous in aquatic environments, and playing multiple key roles in water treatment) (Lutze et al., 2015a; Varanasi et al., 2018; Leenheer and Croué, 2003). Briefly, the presence of DOM is known to decrease the removal efficiency of TOrCs due to its radical scavenging effect. Also, DOM transformation or removal can control disinfection byproducts formation or membrane fouling by applying $SO_4^{\bullet-}$-based AOPs as a pretreatment strategy (Chu et al., 2015; Xie et al., 2015; Cheng et al., 2017; Tian et al., 2018). Therefore, an advanced knowledge on $SO_4^{\bullet-}$-induced reactivity and transformation of DOM is crucial to different water treatment processes considering its ubiquitous presence and the promising

* Corresponding author. , Institut de Chimie des Milieux et des Materiaux IC2MP UMR 7285 CNRS, Universite de Poitiers, France
E-mail address: jean.philippe.croue@univ-poitiers.fr (J.-P. Croue).

https://doi.org/10.1016/j.watres.2019.07.013
0043-1354/

application of $SO_4^{\bullet-}$-based techniques.

The reactivity of DOM with oxidants such as chlorine, ozone, and $^{\bullet}OH$ has been extensively investigated. The difference in reactivity (i.e., faster reaction rate at the initial oxidation phase as compared to subsequent reaction phases) of different DOM isolates has been previously correlated with their structural variability and complexity (Chon et al., 2015; Westerhoff et al., 2004). Interestingly, while $^{\bullet}OH$ non-selectively reacts with target substances, $SO_4^{\bullet-}$ mainly reacts with electron rich aromatic or conjugated double bond moieties (Varanasi et al., 2018). This reactive DOM fraction has been termed as chromophoric dissolved organic matter (CDOM) due to its light absorbing property (Leenheer and Croué, 2003; Lee et al., 2006). Therefore, the degradation rate of CDOM, as measured by ultraviolet absorbance at 254 nm (UVA_{254}) (Westerhoff et al., 2007), could be used to determine its reactivity to $SO_4^{\bullet-}$.

A detailed study on the transformation of DOM, as a result of its reactivity to $SO_4^{\bullet-}$, remains challenging due to its structural complexity and a lack of analytical techniques. Alternatively, traditional DOM characterization techniques could be applied to provide some insights into $SO_4^{\bullet-}$-induced changes of typical DOM characteristics, e.g., electron donating capacity (EDC), optical property (chromophoric or fluorescent property), molecular weight, or organic content (Li et al., 2016; Wang et al., 2017). For instance, an investigation on the transformation of DOM with $^{\bullet}OH$ was conducted by tracking the changes in chromophoric and fluorescent properties (Sarathy and Mohseni, 2008). Specifically, the partial oxidation (i.e., no significant carbon removal) of DOM led to the breakdown of larger molecules, ring open of aromatic structures and the formation of small organics. Interestingly, due to the favorable decarboxylation mechanism driven by $SO_4^{\bullet-}$, a higher DOM mineralization would be expected (Varanasi et al., 2018; Madhavan et al., 1978).

To fill this knowledge gap, the objective of this study was to investigate the reactivity and transformation of CDOM with $SO_4^{\bullet-}$. The reactivity of CDOM was studied by following the decrease of its UVA_{254} with time. A second order rate constant of fast reacting CDOM was calculated based on an established correlation between UVA_{254} and radical exposure. By recording the changes in UVA_{254}, electron donating capacity (EDC), fluorescence intensity (FI), and total organic carbon (TOC), information on CDOM transformation was obtained. A Co(II)-activated peroxymonosulfate (PMS) process was used for the production of $SO_4^{\bullet-}$ due to its high efficiency and simplicity. Four well characterized hydrophobic DOM fractions of different origins and characteristics were selected as model CDOM. This selection of organic isolates obtained from various sources shaping different characters represents a significant advance compared to model organics used in previous investigations.

2. Materials and method

2.1. Chemical reagents and DOM fractions

Peroxomonosufate (Oxone, $KHSO_5 \cdot 0.5KHSO_4 \cdot 0.5K_2SO_4$), 2,2′-azinobis (3-ethylbenzothiazoline-6-sulfonic acid) diammonium salt (ABTS; ≥98%), cobalt(II) sulfate (≥99.0%), sodium tetraborate (≥99.5%), ethanol (≥99.5%), and *tert*-butanol (pure) were purchased from Sigma-Aldrich and prepared with Ultrapure water (PURELAB Ultra, ELGA). Sulfuric acid of HPLC grade and sodium thiosulfate ($Na_2S_2O_3$) were purchased from UNIVAR. *p*-chlorobenzoic acid (pCBA, Acros Organics) was dissolved in ultrapure water to a concentration of 0.2 mM and used as a stock solution. A PMS stock solution of a high concentration (10 mM) was prepared and kept at 4 °C due to its instability. The concentration of the stock solution was monitored on a daily basis prior to use.

Four DOM fractions previously isolated and characterized were selected for this study: Hydrophobic acids (i.e., DOM adsorbed onto XAD-8® resin at acid pH and eluted with sodium hydroxide) extracted from Suwannee River water (S-HPOA, USA) and Beaufort Reservoir (B-HPOA, France); hydrophobic DOM (i.e., similar protocol using a mixture of water and acetonitrile for resin elution) isolated from Ribou Reservoir NOM (R-HPO, France) and Colorado River (C-HPO, USA). The characteristics of the DOM isolates were summarized in Table S1.

2.2. Experimental setup and procedures

Experiments were conducted in 40-mL amber glass vials with Teflon caps. A pre-determined amount of Co(II) as well as DOM stock solution were added into the 10 mM borate buffer to obtain a final composition of 3.90 ± 0.11 mg C/L of DOM and 1 μM of Co(II) at pH 8. Instead of phosphate buffer, tetraborate was used as a buffer solution due to the reported complexing ability of the former with cobalt. A pH 8 buffer was used due to its improved buffering capacity upon the addition of PMS at high concentrations.

The experiments for CDOM reaction kinetics were started by introducing 1 mM PMS. The use of a high initial PMS concentration would allow for a study under both low and high PMS exposure conditions, representative of different water treatment processes. Ethanol and *tert*-butanol at different concentrations (1 or 10 mM) were used as radical quenching agents, while *p*CBA (10 μM) was used as a model compound to quantify primary reactive species. Samples were collected at specified time intervals and subjected to immediate measurement of PMS residual and UV absorbance at 254 nm (UVA_{254}) without the addition of quenching agent. The value of UVA_{254} was further corrected by subtracting the interferences from borate buffer (i.e., including H_2SO_4 for pH adjustment), $CoSO_4$, and PMS. Also, the contribution of PMS at each sampling time was calculated based on the residual PMS concentration and its ε_{254nm} measured in this study (12.3 $M^{-1}cm^{-1}$). For samples subjected to *p*CBA analysis, the reaction was stopped by adding 0.1 mL of ethanol (10 M) to 0.9 mL of sample. Sodium thiosulfate was found inefficient in quenching residual PMS with concentrations as high as 600 mM.

In order to avoid the interference of quenchers on Electron Donating Capacity (EDC) measurements, a new set of experiments was performed by using various initial PMS concentrations (i.e., from 0.00 to 1.00 mM) to achieve experimental conditions with different PMS exposures. PMS residual was periodically monitored, and all samples were analyzed after complete PMS consumption. All experiments were performed at room temperature (20 °C) in glass bottles installed on a rotary shaker (Ika-Werke GMBH & Co. (KG), Labortechnik KS250 Basic) operated at 500 rpm.

2.3. Analytical methods

2.3.1. Analysis of residual PMS

The concentration of PMS was measured by an $ABTS^{\bullet+}$-based method described elsewhere (Zhang et al., 2016). In this method, $ABTS^{\bullet+}$ is generated during the oxidation of ABTS by sulfate radical produced through the catalytic transformation of PMS, and then it was spectrophotometrically measured. Briefly, a solution containing 0.5 mL of ABTS (20 mM), 0.2 mL of $CoSO_4$ (20 mM), 10 mL of H_2SO_4 (2%), and 1 mL of water sample was well mixed and measured at a 734 nm wavelength with a spectrophotometer (Cary 60, Agilent). The calibration curve for PMS determination was shown in Fig. S1. A high concentration of $CoSO_4$ (20 mM) was applied to accelerate the catalytic decomposition of PMS. However, this interference has been taken into consideration with the measurement of a blank sample with no PMS addition, as suggested by

the calibration curve in Fig. S1. Also, a background DOM would not be influential due to a measurement recorded at 734 nm.

2.3.2. Characterization of DOM transformation

The EDC of DOM samples was analysed based on a method developed by Chon et al. (2015). Briefly, a size exclusion chromatography (SEC) coupled with post column reaction was used, where $ABTS^{\bullet+}$ was produced by the oxidation of ABTS with sodium persulfate in acidic environment. A TOYOPEARL HW-50S column (8 mm × 30 cm) was selected for SEC using a 50 mM borate eluent (pH 7.8) at a flow rate of 0.2 mL/min. The post-column injection of $ABTS^{\bullet+}$ solution was operated at 0.05 mL/min from the helium pressurised generator. The reaction coil was connected to two UV detectors positioned in series (Agilent 1100 series, USA): the first one recording UV absorbance of DOM at 254 nm, and the second one recording the signal for ABTS/$ABTS^{\bullet+}$ at 405 nm.

A Cary 60 spectrophotometer (Agilent, USA) was used to collect absorbance data or to record the UV−vis spectra from 200 nm to 800 nm in 1 cm path length quartz cell. The TOC concentration of each sample was measured with a Shimadzu TOC-L analyser (SHIDMAZU, Japan).

Fluorescence excitation and emission matrices (EEMs) were obtained using a Fluorescence spectrometer (Cary Eclipse, Varian). The operating parameters were adjusted based on the method from Chen et al. (2003). Briefly, the scan rate and excitation or emission slit bandwidth were set at 600 nm/min and 5 nm, respectively. The spectra were recorded by scanning an emission spectra from 290 nm to 550 nm at a 5 nm increment with the excitation wavelength ranging from 220 nm to 400 nm at a 5 nm increment.

The concentration of *p*CBA was measured with a HPLC unit equipped with a UV detector (Agilent 1100 series, USA) recording absorbance at 238 nm and with a 250 mm*4.6 mm C18 5-μm reverse phase column (Alltima™, GRACE). The mobile phase consisted of 60% methanol and 40% phosphoric acid (0.1%, V/V). The *p*CBA calibration curve was built using gradually diluted stock solution.

3. Results and discussion

3.1. Biphasic decrease of CDOM in Co(II)/PMS system

The reaction of CDOM with PMS led to an average decrease of 11% in UVA_{254} within 60 min (Fig. S2). However, the decrease of UVA_{254} was remarkably faster in the presence of both PMS and Co(II) (Fig. 1). Approximately 55%−70% decrease in UVA_{254} (depending on the DOM fraction) was observed in Co(II)-catalyzed PMS system within 60 min. This enhanced reaction was caused by the generation of reactive species (e.g., $SO_4^{\bullet-}$) in the Co(II)/PMS system, while the slight UVA_{254} decrease in the absence of Co(II) catalyst was probably due to the reaction of quinones with PMS as previously reported (Zhou et al., 2015). The occurrence of quinones within humic substances has been widely acknowledged (Cory and McKnight, 2005).

Noticeably, a fast and slow reaction phase could be distinguished for all DOM fractions throughout the oxidation process (Fig. 1). Specifically, the pseudo-first-order rate constants of the fast reaction phase were 4.2−6.9 times higher than the rate constants of the slower reaction phase. These results showed a significant difference in the reactivity of CDOM with $SO_4^{\bullet-}$ due to the heterogeneous structural property of the organic matter isolates. It has been previously reported that aromatic structures substituted with electron donating groups (i.e., −OH, $-NH_3$, $-OCH_3$) exhibited higher reactivity to $SO_4^{\bullet-}$ (Luo et al., 2017); these structures could represent the main contributor to the fast reacting CDOM (i.e., $CDOM_{fast}$). The slow reacting CDOM (i.e., $CDOM_{slow}$) might include

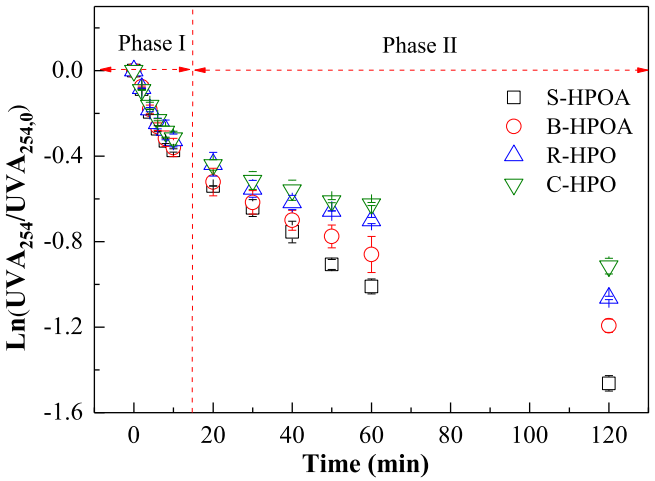

Fig. 1. UVA_{254} decrease of different DOM fractions in Co(II)/PMS system as a function of time. Conditions: $[PMS]_0 = 1.0$ mM; Co(II) = 1.0 μM; DOM = 3.90 ± 0.11 mgC/L; pH = 8.00 ± 0.05 (10 mM borate buffer); T = 20 °C.

lower electron density moieties from the original CDOM constituents as well as the oxidation products of $CDOM_{fast}$ (Xiao et al., 2015; Zhang et al., 2012).

The influence of the aromatic character of the DOM fractions on their reactivity with $SO_4^{\bullet-}$ was highly expected based on previous findings (Westerhoff et al., 2004; Luo et al., 2017). However, the difference in reactivity among the four DOM fractions was more significant during the slow reaction phase. The pseudo-first-order reaction rates of $CDOM_{slow}$ (i.e., $\ln(UVA_{254}/UVA_{254,0})$ versus reaction time) were calculated as 1.20×10^{-2}, 0.84×10^{-2}, 0.63×10^{-2}, and 0.46×10^{-2} min^{-1} for S-HPOA, B-HPOA, R-HPO and C-HPO, respectively. These $CDOM_{slow}$ reactivities linearly increased with the SUVA values as shown in Fig. S3. The $CDOM_{fast}$ reactivity to $SO_4^{\bullet-}$ of the four DOM fractions was further discussed in the following sections.

3.2. Evaluation of sulfate radical production

Anipsitakis and Dionysiou (2003) reported the predominant role of $SO_4^{\bullet-}$ (eq. (1)) over $^{\bullet}OH$ in Co(II)-catalyzed PMS systems at pH 7. Because a pH 8 may promote a higher production of $^{\bullet}OH$ (eq. (2)), the identification of major oxidizing species in the current system was conducted by following the degradation of *p*CBA as a probe compound under different scavenging conditions (Lutze et al., 2015b). The second-order rate constants of *p*CBA and radical scavengers (i.e., *t*-BuOH and EtOH) with $^{\bullet}OH$ and $SO_4^{\bullet-}$ were summarized in Table S3. When 10 mM of radical scavenger (i.e., *t*-BuOH or EtOH, at a molar ratio of 1000:1 versus *p*CBA) was applied, the *p*CBA removal efficiency was decreased by approximately 10% in the presence of *t*-BuOH; while almost no *p*CBA decrease was observed with the addition of EtOH (Fig. S4). Quantitatively, the ratio of the measured concentration of $^{\bullet}OH$ to $SO_4^{\bullet-}$was lower than 3%. These results indicated that $SO_4^{\bullet-}$ was the predominant reactive species at pH 8. This is probably due to the competition for $SO_4^{\bullet-}$ by either pCBA (3.6×10^8 $M^{-1}s^{-1}$) or scavengers (i.e., DOM fractions, up to 10^8 $M^{-1}s^{-1}$ as discussed below), leading to the unfavorable production of $^{\bullet}OH$ (eq (2)).

$$HSO_5^- + Co^{2+} = SO_4^{\bullet-} + Co^{3+} + OH^- \quad (1)$$

$$SO_4^{\bullet-} + OH^- = SO_4^{2-} + {}^{\bullet}OH \left(k_{SO_4^{\bullet-},\, OH^-} = 6.5 \times 10^7 M^{-1}s^{-1}\right) \quad (2)$$

$$HSO_5^- + Co^{3+} = SO_5^{\bullet-} + Co^{2+} + H^+ \quad (3)$$

Therefore, the production of $SO_4^{\bullet-}$ was investigated following the R_{ct} concept and the analysis of *p*CBA decay. R_{ct} (i.e., the ratio of radical exposure to oxidant exposure) (Elovitz and von Gunten, 1999) was used to present the production of $SO_4^{\bullet-}$ with PMS exposure (eq. (4)). According to Elovitz and von Gunten (1999), the consumption of radicals by a probe compound (P) (e.g., *p*CBA in the current study) is considered insignificant as compared to major radical scavengers (S) (e.g., DOM in current study) if the probe compound is present at a considerably low concentration (i.e., $k_P[P] \ll k_S[S]$, where k_P and k_S represents the rate constants of the probe compound and major radical scavengers with radicals, respectively). Therefore, a low *p*CBA concentration (i.e., 1 μM) was applied to ensure an insignificant radical consumption by *p*CBA as compared to DOM. Specifically, $k_{pCBA}[pCBA]$ was calculated as approximately 1.4% of $k_{DOM}[DOM]$ under the current experimental condition, where k_{pCBA} and k_{DOM} represent the second order rate constants of *p*CBA ($3.6 \times 10^8\ M^{-1}s^{-1}$) and DOM ($6.8 \times 10^3$ $LmgC^{-1}s^{-1}$) with $SO_4^{\bullet-}$, respectively. The R_{ct} value was only studied for the first 10 min of the reaction. $CDOM_{fast}$ was observed reactive within this timeframe (Fig. 1). The conversion from reaction time to PMS exposure was illustrated in Table S4.

Although no noticeable interference was observed with UVA_{254} or EDC measurements, the rate of catalytic PMS decomposition decreased (Fig. S5) due to the formation of cobalt-DOM complex. For instance, a 57% PMS decomposition was observed within 60 min in the DOM-free system. However, the PMS decomposition values for S-HPOA-, B-HPOA-, R-HPO-, and C-HPO-containing system were 41%, 43%, 40%, and 43%, respectively. Specifically, approximately 80% of Co(II) was calculated as forming complexes with DOM under the current experimental conditions using the NICA-Donnan model with the constants adapted from Milne et al. (2003). In DOM-containing solutions with the addition of *p*CBA as probe compound, PMS decomposed following a pseudo-first-order reaction (Fig. S6a), as described by (eq. (5)), and *k* (i.e., pseudo-first-order rate constant) was measured as approximately $3.0 \times 10^{-4}s^{-1}$ independent of DOM origins. The influence of *p*CBA addition (1 μM) on PMS decomposition was negligible. For instance, the averaged PMS residual measured in different DOM-containing systems within 10 min was 80% in the absence of *p*CBA (Fig. S5) and 79% in the presence of *p*CBA (Fig. S6a). The determined rate (within 10 min) was predominantly contributed by a catalytic decomposition since self-decomposition of PMS was found negligible within 2 h at room temperature (20 °C). The degradation of *p*CBA (Fig. S6b) caused by $SO_4^{\bullet-}$ was described by eqs. (6) and (7). By combining eqs. (4) and (5), *p*CBA degradation could be described using the R_{ct} concept (eq. (8)).

$$R_{ct} = \frac{\int_0^t [SO_4^{\bullet-}]\,dt}{\int_0^t [PMS]\,dt} \quad (4)$$

$$[PMS] = [PMS]_0 e^{-kt} \quad (5)$$

$$-\frac{d[pCBA]}{dt} = k_{SO_4^{\bullet-},\, pCBA}[pCBA]\,[SO_4^{\bullet-}] \quad (6)$$

$$\ln\frac{[pCBA]}{[pCBA]_0} = -k_{SO_4^{\bullet-},\, pCBA}\int_0^t [SO_4^{\bullet-}]\,dt \quad (7)$$

$$\ln\frac{[pCBA]}{[pCBA]_0} = -k_{SO_4^{\bullet-},\, pCBA}R_{ct}[PMS]_0\int_0^t e^{-kt}dt \quad (8)$$

By plotting ln ($pCBA/pCBA_0$) versus PMS exposure, linear correlations were observed as a function of PMS exposures (Fig. 2). The R_{ct} value at PMS exposures higher than 0.1 M s (i.e. a reaction time of 2–10 min, Table S4) for each system was determined from the slope of the linear regression line (Fig. 2) and listed in Table 1; while the higher R_{ct} values at PMS exposures lower than 0.1 M s (i.e. a reaction time of 0–2 min, Table S4) were shown in Fig. S7. Higher R_{ct} values at the initial oxidation stage (PMS exposure < 0.1 M s, results discussed in section 3.4.1) have also been reported during the ozonation of surface waters (Elovitz and von Gunten, 1999). The change of R_{ct} in the current study was likely due to the Co(II) regeneration process. Specifically, the conversion of Co(II) to Co(III) with a precipitate formation of the latter has been considered as a probable explanation for the slowing down of the catalytic rate with time at pH above 5.9 (Zhang and Edwards, 1992). With a pH of 8 used in this study, Co(III) might have also precipitated out as $Co(OH)_3$ ($K_{sp} = 1.6 \times 10^{-44}$), leading to the retardation of the regeneration process and consequently to a slower $SO_4^{\bullet-}$ production. Moreover, the additional PMS consumption during the regeneration of Co(II) (eq. (3)), which inefficiently produced $SO_5^{\bullet-}$ (Neta et al., 1988), would also lead to a decreased R_{ct}. A change in Co(II) catalytic behavior at different pH probably associated with Co(III) precipitation at higher pH has also been observed in previous studies. For instance, the degradation rate of 2,4-DCP in Co(II)/PMS system slowed down with reaction time at pH 7 (Anipsitakis et al., 2005), while it remained unaffected at pH 2 (Anipsitakis and Dionysiou, 2003). Considering that no enhanced UVA_{254} decrease (explained in Section 3.4.1) was observed (Fig. 1) in contrast to the significantly higher *p*CBA degradation (Fig. S6b) at the initial oxidation stage (i.e., PMS exposure lower than 0.1 M s), the relatively lower R_{ct} values (Table 1) determined after the initial short stage were used in the analysis of the following section.

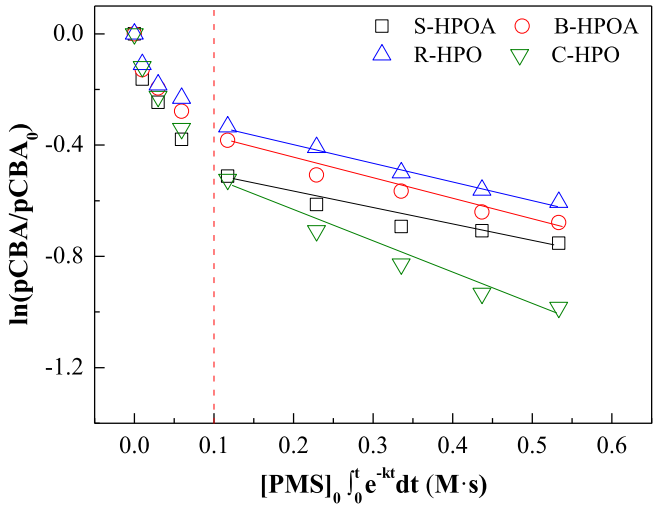

Fig. 2. Correlation between *p*CBA decay and PMS exposure in Co(II)/PMS system with different DOM fractions. Conditions: $[PMS]_0 = 1.00$ mM; Co(II) = 1.00 μM; $[pCBA]_0 = 1.00$ μM; DOM = 3.90 ± 0.11 mgC/L; pH = 8.00 ± 0.05 (10 mM borate buffer); T = 20 °C.

Table 1
R_{ct} values in different DOM-containing systems under PMS exposure higher than 0.1 M s ($ln(pCBA/pCBA_0) = -A([PMS]_0 \int_0^t e^{-kt}dt) + B$, R^2; $R^{ct} = A/k_{SO_4^{\bullet-},pCBA}$).

DOM fraction	A	R_{ct}	R^2
S-HPOA	0.588	1.55×10^{-9}	0.935
B-HPOA	0.701	1.95×10^{-9}	0.970
R-HPO	0.670	1.86×10^{-9}	0.990
C-HPO	1.107	3.08×10^{-9}	0.968

3.3. Reactivity of $CDOM_{fast}$ to $SO_4^{\bullet-}$ and its application

Following the procedures for establishing a relationship between ln ($pCBA/pCBA_0$) and PMS exposure (eq. (8)), i.e., obtained by combining eq. (4), eq. (5) and eq. (7)), a similar correlation was also established between $\ln(UVA_{254}/UVA_{254,0})$ of $CDOM_{fast}$ and PMS exposure (eq. (9)). This correlation was found linear when $\ln(UVA_{254}/UVA_{254,0})$ of $CDOM_{fast}$ was plotted against PMS exposure for all DOM fractions (Fig. 3). The good linearity allowed the calculation of the reaction rate constant of $CDOM_{fast}$ with $SO_4^{\bullet-}$ using the R_{ct} value determined in Section 3.2.

$$\ln\frac{[UVA_{254}]}{[UVA_{254}]_0} = -k_{SO_4^{\bullet-},CDOM}R_{ct}[PMS]^0\int_0^t e^{-kt}dt \quad (9)$$

Interestingly, the reaction rate constants of $CDOM_{fast}$ for all DOM fractions were at the same order of magnitude. The highest $CDOM_{fast}$ value was recorded for S-HPOA ($4.59 \times 10^8\ M^{-1}s^{-1}$), also exhibiting the highest SUVA (4.78). The lowest $CDOM_{fast}$ value was observed for C-HPO ($1.99 \times 10^8\ M^{-1}s^{-1}$), also showing lowest SUVA (2.14). However, B-HPOA (SUVA: 4.06) showed a lower k value than R-HPO (SUVA: 3.22), i.e., $3.04 \times 10^8\ M^{-1}s^{-1}$ versus $3.48 \times 10^8\ M^{-1}s^{-1}$, respectively. Therefore, the correlation between the reactivity of $CDOM_{fast}$ and SUVA of the corresponding DOM fraction would need additional investigation by including a larger pool of DOM fractions. These reaction rate constants were one order of magnitude higher than the data previously reported (i.e., $\sim 10^7 M_C^{-1}s^{-1}$). For instance, Lutz et al. (2015a) observed a rate of $6.8 \times 10^3\ LmgC^{-1}s^{-1}$ for humic acid (Depur from Carl Roth) using an indirect kinetic competition method; while Zhou et al. (2017) recorded a rate of $1.86 \times 10^3\ LmgC^{-1}s^{-1}$ for Suwannee River fulvic acid using a direct laser flash photolysis method. The difference could be attributed to the fact that the value in this study was only measured for the conceptually isolated fast reacting moieties (i.e., $CDOM_{fast}$) rather than for the bulk DOM (i.e., a combination of both fast and slow reacting moieties). However, the value was one order of magnitude lower than those reported for aromatic compounds ($\sim 10^9\ M^{-1}s^{-1}$) (Neta et al., 1977; Fischer and Radom, 2001). This difference would be the result of stronger electrosteric repulsion between $SO_4^{\bullet-}$ and structurally complex DOM as compared to simpler organic compounds. The higher reactivity of sulfate radicals to $CDOM_{fast}$ than to OH^- ($\sim 10^7 M^{-1}s^{-1}$) was expected to lead to an insignificant production of $^{\bullet}OH$ (eq. (2)) due to its unfavorable formation kinetics. In addition, $CDOM_{fast}$ would be preferred to bulk DOM when evaluating the scavenging property of dissolved organic matter in $SO_4^{\bullet-}$-based AOPs under lower PMS exposures, where $CDOM_{fast}$ was the major reactive moieties (Fig. 1).

The use of UVA_{254} as a surrogate indicator for the assessment of TOrCs removal efficiency has been extensively studied in ozone- and $^{\bullet}OH$-based AOPs (Gerrity et al., 2012; Rosario-Ortiz et al., 2010; Li et al., 2017). This finding could also support its application in $SO_4^{\bullet-}$-based water treatment processes. The study on TOrCs removal efficiency could be achieved using either: i) the kinetics with second order reaction constants of TOrCs and radical exposure (eq. (10)), or ii) the correlation established between UVA_{254}

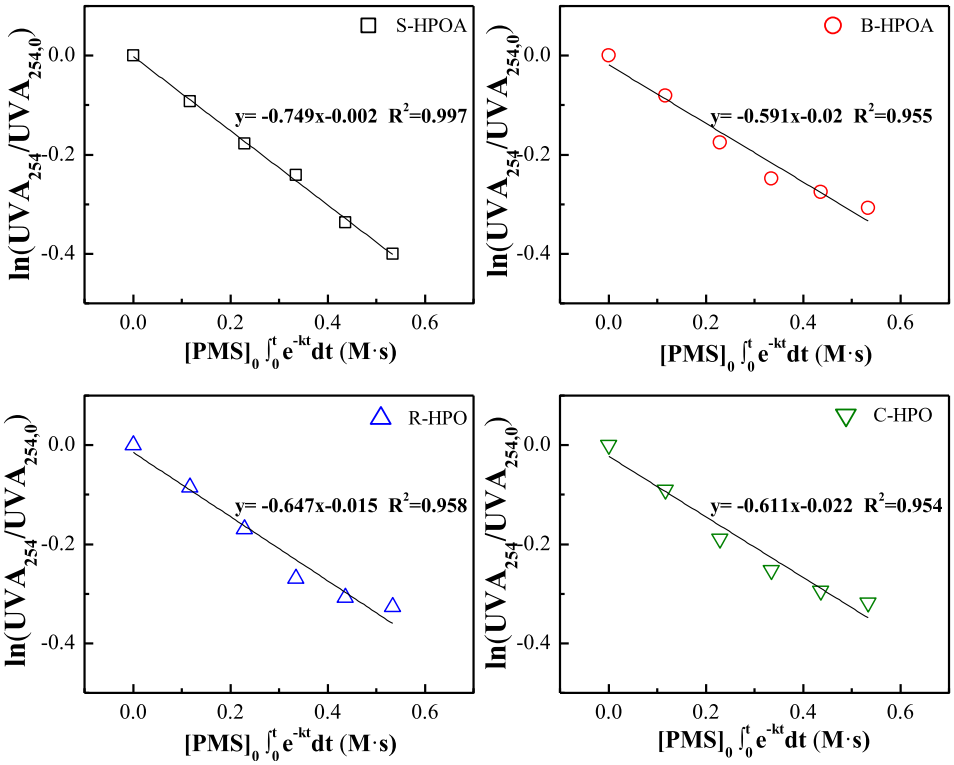

Fig. 3. Correlation between $CDOM_{fast}$ decrease and PMS exposure in Co(II)/PMS system. Conditions: $[PMS]_0 = 1.00$ mM; Co(II) = 1.00 μM; $[pCBA]_0 = 1.00$ μM; DOM = 3.90 ± 0.11 mgC/L; pH = 8.00 ± 0.05(10 mM borate buffer); T = 20 °C.

decrease and contaminants removal (eq. (11)).

$$\ln\frac{[TOrCs]}{[TOrCs]_0} = -k_{SO_4^{\bullet-},\,TrOCs}\int_0^t SO_4^{\bullet-}\,dt$$
$$= -k_{SO_4^{\bullet-},\,TrOCs}\ln\frac{[UVA_{254}]}{[UVA_{254}]_0}\Big/ - k_{SO_4^{\bullet-},\,CDOM} \quad (10)$$

$$\ln\frac{[TOrCs]}{[TOrCs]_0} = Slope \times \ln\frac{[UVA_{254}]}{[UVA_{254}]_0} + Intercept \quad (11)$$

As compared to the direct measurement of TOrCs in a full-scale water treatment plant, the indirect monitoring of UV absorbing parameters using spectrophotometer would require lower capital/operating cost as well as time input. Especially, with the use of an on-line spectrophotometer, a quick track of the oxidation efficiency and consequently a rapid adjustment (i.e., oxidant dose or contact time) could also be expected. However, different correlation models should be established for different TOrCs due to the discrepancy in their reactivity. The successful application of this correlation could also be impacted by the fluctuation of water matrices (e.g., HCO_3^-, NO_3^-, or Cl^-) or temperature due to seasonal changes.

The use of UV absorbing indices of humic substances in combination with their fluorescence properties has also been suggested as indicators in ozone-based water treatment processes (Li et al., 2017). However, similar decreasing trend was observed in the current study between UVA_{254} and fluorescence intensity with increasing PMS concentration (Text S1). Consequently, the UVA_{254} parameter was sufficient as a single process indicator in this $SO_4^{\bullet-}$-based oxidation system.

3.4. Sulfate radical-induced CDOM transformation

3.4.1. EDC decrease as a function of PMS exposures

Electron donating capacity (EDC) associated with the presence of phenolic structures with different degree of substitution has been previously reported for aquatic humic substances (Aeschbacher et al., 2012). The change in EDC (Fig. S8) was studied for each DOM fraction under various PMS exposures. The different PMS exposures were obtained by applying varying initial PMS concentrations for the same contact time (i.e., 20 h) and the calculation of the PMS exposures was detailed in Text S2, SI. In addition, the changes in normalized EDC and UVA_{254} (Fig. S9) of the four DOM fractions were plotted in Fig. 4. This figure shows that for PMS exposures lower than 0.1 M s (Area a_1), an average of 54% decrease of EDC was recorded when only a 30% decrease of UVA_{254} was observed. For PMS exposures higher than 0.1 M s (Area b), the averaged normalized UVA_{254} decreased from 70% to 13% (i.e., a 57% decrease), whereas the averaged normalized EDC decreased from 46% to 7% (i.e., a 39% decrease). The larger decrease of EDC than UVA_{254} at PMS exposure lower than 0.1 M s in this system indicated that the initial phase of $SO_4^{\bullet-}$ reaction was the oxidation of phenolics into quinone-type structures with similar chromophoric properties (Ramseier and Gunten, 2009). This reaction is thermodynamically favourable considering the very low oxidation potential of phenolic structures (0.153–0.620 V) (Bortolomeazzi et al., 2007) and the strong reduction potential of sulfate radicals (2.5–3.1V) (Anipsitakis and Dionysiou, 2003). A similar observation has been previously reported during the treatment of humic substances by ClO_2 or HClO, where hydroquinone or catechol moieties (i.e., major EDC contributors (Chon et al., 2015)) were proposed as oxidized by HClO through electron transfer rather than electrophilic substitution (Wenk et al., 2013). Interestingly, a more

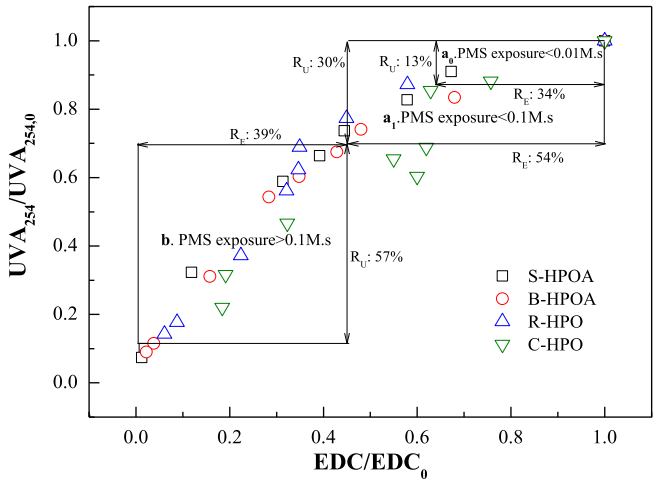

Fig. 4. Correlation between normalized UVA_{254} and EDC decrease of different DOM fractions in Co(II)/PMS reaction system. Conditions: PMS exposure = 0.00–8.04 M s; Co(II) = 1.00 μM; DOM = 3.90 ± 0.11 mgC/L; pH = 8.00 ± 0.05 (10 mM borate buffer); T = 20 °C. Areas a_0, a_1, and b illustrated the results obtained with a PMS exposure lower than 0.01, lower than 0.1, and larger than 0.1 M s, respectively. R_E and R_U represented the normalized removal efficiency in EDC and UVA_{254}.

pronounced decrease in EDC than in UVA_{254} was observed with a PMS exposure lower than 0.01 M s (Area a_0, Fig. 4), which was probably caused by the relatively higher R_{ct} observed under this condition (Fig. S7).

Due to a major $SO_4^{\bullet-}$ consumption by the moieties with EDC at the initial oxidation phase (i.e., PMS exposure < 0.1 M s), a UVA_{254} decrease was not enhanced even under higher radical exposure (i.e., higher R_{ct}) (Fig. 3). This result supported the selection of lower R_{ct} values (Fig. 2) in the calculation of the second-order rate constants of $CDOM_{fast}$ with $SO_4^{\bullet-}$ as described in section 3.3.

3.4.2. TOC removal efficiency at various PMS exposures

In order to further explore the transformation of CDOM by sulfate radicals, the TOC content of the solution under different PMS exposures was measured. A significant TOC removal, 64%, 63%, 56%, 49% for S-HPOA, B-HPOA, R-HPO and C-HPO, respectively (i.e., 58% in average), was observed under a PMS exposure of 8.04 M s (Fig. S10). The relationship between UVA_{254} decrease and TOC removal was established and shown in Fig. 5. Interestingly, the TOC removal was minor (i.e., less 10%) during the depletion of the UV absorbance of $CDOM_{fast}$ (i.e., UVA_{254} decrease within 50%, as indicated by the red dashed line in Fig. 5). However, the decrease in the chromophoric property of $CDOM_{slow}$ (i.e., observed when UVA_{254} decrease was larger than 50%, right side of the red dashed line in Fig. 5) led to a considerable TOC removal. These results indicated that the reaction of $CDOM_{fast}$ would mainly lead to the breakdown of complex aromatic structures into small molecular weight fractions with insignificant mineralization. This transformation from larger molecules to smaller ones was evidenced by the blue shift or band contraction (Chen et al., 2002) in fluorescence emission spectra (Fig. 6). Specifically, the decrease in the bandwidth at 1/2 maximum fluorescence intensity was calculated as 24 nm, 24 nm, 33 nm, and 88 nm for S-HPOA, B-HPOA, R-HPO, and C-HPO, respectively. In contrast, the reaction of $CDOM_{slow}$ would mainly undergo through decarboxylation, which directly led to the observed carbon removal.

Interestingly, a good linearity between UVA_{254} decrease and TOC removal during the $CDOM_{slow}$ decrease was observed (Fig. 5). These results indicated that the change in $CDOM_{slow}$ could be used in the prediction of TOC removal for surface water during $SO_4^{\bullet-}$-

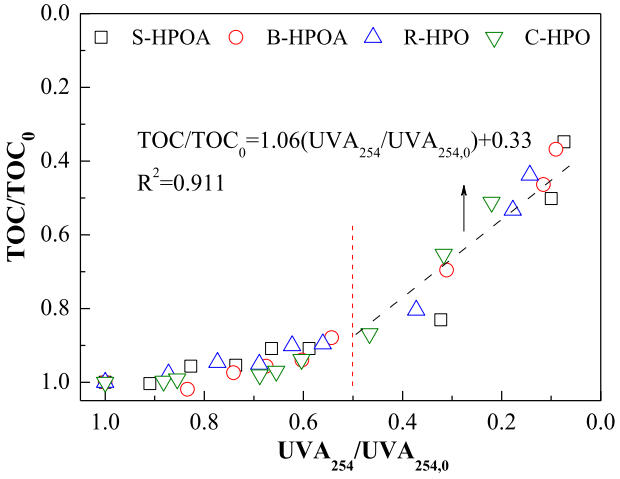

Fig. 5. TOC removal as a function of UVA_{254} decrease. Conditions: PMS exposure = 0.00–8.04 M s; Co(II) = 1.00 μM; DOM = 3.90 ± 0.11 mgC/L; pH = 8.00 ± 0.05 (10 mM borate buffer); T = 20 °C. Red dashed line was drawn to differentiate the correlation between $CDOM_{fast}$ and $CDOM_{slow}$ with TOC removal. (For interpretation of the references to colour in this figure legend, the reader is referred to the Web version of this article.)

3.4.3. Evolution of CDOM transformation with sulfate radical

Based on the findings of this study (i.e., results obtained with the current characterization techniques), the evolution of the transformation of CDOM by sulfate radicals was summarized in Fig. 7. The $SO_4^{\bullet-}$-induced reaction of $CDOM_{fast}$, (i.e., electron donating group substituted aromatic structures) was mainly initiated through single electron transfer or addition. The depletion of EDC would initially take place through the electron transfer from phenolic hydroxyl groups to sulfate radical as suggested by Reaction 1. Reaction 2 would produce hydroxylated C-centered radical cations and consequently lead to the formation of ring cleavage products (Anipsitakis et al., 2006). Remarkably, Reaction 4 would take place due to the high electron density at R_3 site leading to the formation of smaller fluorescent molecules, as suggested by the blue shift of fluorescence emission spectra (Fig. 6). The production of smaller molecules from complex structures could also be evidenced by the increased fluorescence signal (Fig. S13) at lower PMS exposure, as the smaller aromatic moieties would be more fluorescent due to weaker intramolecular quenching effect. The decarboxylation of carboxyl groups (Reaction 3), i.e., newly formed or originally incorporated within DOM structures, would be the main reaction mechanism of $CDOM_{slow}$ transformation (Madhavan et al., 1978) leading to a significant removal of TOC. However, a

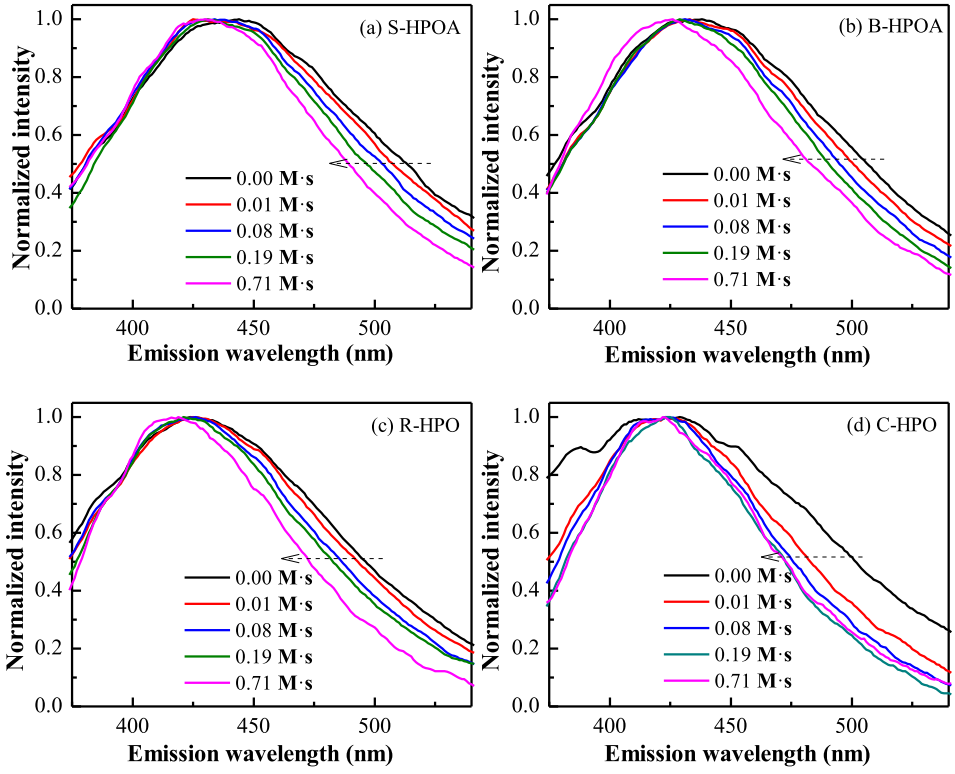

Fig. 6. Normalized emission spectra by its respective maximum fluorescence intensity of (a) S-HPOA, (b) B-HPOA, (d) R-HPO, and (d) C-HPO at an excitation wavelength of 230 nm. The legend in each figure represented various PMS exposures.

based treatment. This may include water treatment processes targeting the removal of organics, e.g., pretreatment for the removal of disinfection byproducts precursors or membranes foulants, membrane cleaning, and the treatment of reverse osmosis concentrates. Nevertheless, under different water matrices this correlation might be affected by pH conditions, or the presence of radical scavengers HCO_3^- or Cl^-.

more detailed study would be highly recommended for the optimization of process conditions for maximum carbon removal.

4. Conclusions

The current study provided systematic information on both the reactivity and fate of CDOM with sulfate radical. DOM fractions

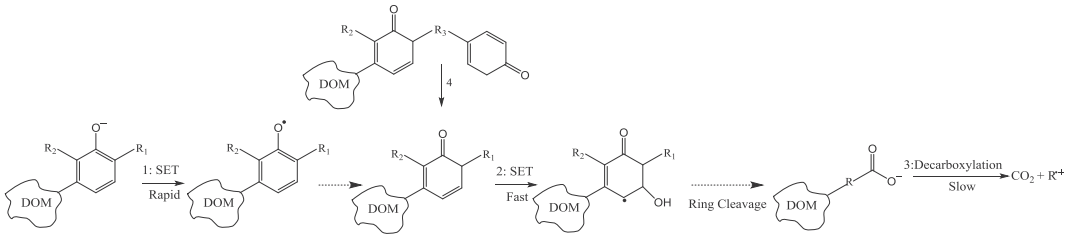

Fig. 7. Proposed pathway of sulfate radical-induced DOM transformation.

with different origins and characteristics were used in this investigation. The main conclusions included:

- Fast and slow reacting CDOM could be distinguished within all DOM fractions. Interestingly, the difference in the reactivity of $CDOM_{fast}$ among different organics were minor, while the reactivity $CDOM_{slow}$ were observed to increase with SUVA.
- The reactivity of $CDOM_{fast}$ to $SO_4^{\bullet-}$ was calculated at an order of $10^8\ M^{-1}s^{-1}$ from the observed linear correlation between $CDOM_{fast}$ decrease and sulfate radical exposure. The correlation also validated the potential application of UVA_{254} as a surrogate indicator for TOrCs removal efficiency.
- A faster decrease of EDC than UVA_{254} at lower PMS exposure indicated a preferred oxidation of phenolic structures (i.e., preferential decrease of Electron Donating Capacity). Afterwards, the oxidation of $CDOM_{fast}$ would proceed with the formation of transient intermediates and ring cleavage products.
- The transformation products of $CDOM_{fast}$ together with the originally less reactive structures, i.e., $CDOM_{slow}$, would undergo slow decarboxylation leading to a significant carbon removal. The linear relationship recorded between $CDOM_{slow}$ reduction and TOC removal could be used to predict carbon removal.

The findings in this work would highly assist in the design and operation of $SO_4^{\bullet-}$- based water treatment processes. Specifically, the scavenging capacity of background DOM could be better evaluated using the calculated reactivity of $CDOM_{fast}$ if the applied PMS exposure would mainly cause changes in $CDOM_{fast}$. Also, the correlation established between CDOM and radical exposure would shed light on the applicability of UVA_{254} as an indicator of TOrCs removal efficiency in $SO_4^{\bullet-}$-based water treatment processes. However, further site-specific studies on the use of UVA_{254} as an indicator are highly needed for its successful application.

$SO_4^{\bullet-}$-based advanced oxidation technique could be developed to address the need for DOM removal in varying water treatment scenarios, e.g., pretreatment for the removal of disinfection by-products precursors or membrane foulants, application of catalytic membrane for organic fouling mitigation, membrane cleaning, or the treatment of reverse osmosis concentrate produced from reclaimed water treatment plants. Also, an increased PMS dose could be applied to increase the reaction rate of $CDOM_{slow}$ and consequently increase carbon removal. In addition, carbon removal efficiency could be simply estimated based on the removal of $CDOM_{slow}$ due to the observed good correlation.

Declaration of interests

The authors declare that they have no known competing financial interests or personal relationships that could have appeared to influence the work reported in this paper.

Acknowledgements

China Scholarship Council (CSC) and Curtin University are acknowledged for providing the CSC-Curtin joint PhD scholarship to Suona Zhang.

Appendix A. Supplementary data

Supplementary data to this article can be found online at https://doi.org/10.1016/j.watres.2019.07.013.

References

Aeschbacher, M., Graf, C., Schwarzenbach, R.P., Sander, M., 2012. Antioxidant properties of humic substances. Environ. Sci. Technol. 46 (9), 4916–4925.
Anipsitakis, G.P., Dionysiou, D.D., 2003. Degradation of organic contaminants in water with sulfate radicals generated by the conjunction of peroxymonosulfate with cobalt. Environ. Sci. Technol. 37 (20), 4790–4797.
Anipsitakis, G.P., Stathatos, E., Dionysiou, D.D., 2005. Heterogeneous activation of Oxone using $Co_3\ O_4$. J. Phys. Chem. B 109 (27), 13052–13055.
Anipsitakis, G.P., Dionysiou, D.D., Gonzalez, M.A., 2006. Cobalt-mediated activation of peroxymonosulfate and sulfate radical attack on phenolic compounds. Implications of chloride ions. Environ. Sci. Technol. 40 (3), 1000–1007.
Bortolomeazzi, R., Sebastianutto, N., Toniolo, R., Pizzariello, A., 2007. Comparative evaluation of the antioxidant capacity of smoke flavouring phenols by crocin bleaching inhibition, DPPH radical scavenging and oxidation potential. Food Chem. 100 (4), 1481–1489.
Chen, J., Gu, B., LeBoeuf, E.J., Pan, H., Dai, S., 2002. Spectroscopic characterization of the structural and functional properties of natural organic matter fractions. Chemosphere 48 (1), 59–68.
Chen, W., Westerhoff, P., Leenheer, J.A., Booksh, K., 2003. Fluorescence Excitation–Emission matrix regional integration to quantify spectra for dissolved organic matter. Environ. Sci. Technol. 37 (24), 5701–5710.
Cheng, X., Liang, H., Ding, A., Tang, X., Liu, B., Zhu, X., Gan, Z., Wu, D., Li, G., 2017. Ferrous iron/peroxymonosulfate oxidation as a pretreatment for ceramic ultrafiltration membrane: control of natural organic matter fouling and degradation of atrazine. Water Res. 113, 32–41.
Chon, K., Salhi, E., von Gunten, U., 2015. Combination of UV absorbance and electron donating capacity to assess degradation of micropollutants and formation of bromate during ozonation of wastewater effluents. Water Res. 81, 388–397.
Chu, W., Li, D., Gao, N., Templeton, M.R., Tan, C., Gao, Y., 2015. The control of emerging haloacetamide DBP precursors with UV/persulfate treatment. Water Res. 72, 340–348.
Cory, R.M., McKnight, D.M., 2005. Fluorescence spectroscopy reveals ubiquitous presence of oxidized and reduced quinones in dissolved organic matter. Environ. Sci. Technol. 39 (21), 8142–8149.
Elovitz, M.S., von Gunten, U., 1999. Hydroxyl radical/ozone ratios during ozonation processes. I. The Rct concept. Ozone: Sci. Eng. 21 (3), 239–260.
Fischer, H., Radom, L., 2001. Factors controlling the addition of carbon-centered radicals to alkenes—an experimental and theoretical perspective. Angew. Chem. Int. Ed. 40 (8), 1340–1371.
Gerrity, D., Gamage, S., Jones, D., Korshin, G.V., Lee, Y., Pisarenko, A., Trenholm, R.A., von Gunten, U., Wert, E.C., Snyder, S.A., 2012. Development of surrogate correlation models to predict trace organic contaminant oxidation and microbial inactivation during ozonation. Water Res. 46 (19), 6257–6272.
Ghauch, A., Baalbaki, A., Amasha, M., El Asmar, R., Tantawi, O., 2017. Contribution of persulfate in UV-254 nm activated systems for complete degradation of chloramphenicol antibiotic in water. Chem. Eng. J. 317, 1012–1025.
Lee, N., Amy, G., Croue, J.-P., 2006. Low-pressure membrane (MF/UF) fouling associated with allochthonous versus autochthonous natural organic matter. Water Res. 40 (12), 2357–2368.
Leenheer, J.A., Croué, J.-P., 2003. Peer reviewed: characterizing aquatic dissolved organic matter. Environ. Sci. Technol. 37 (1), 18A–26A.
Li, T., Jiang, Y., An, X., Liu, H., Hu, C., Qu, J., 2016. Transformation of humic acid and halogenated byproduct formation in UV-chlorine processes. Water Res. 102,

421–427.
Li, W.-T., Cao, M.-J., Young, T., Ruffino, B., Dodd, M., Li, A.-M., Korshin, G., 2017. Application of UV absorbance and fluorescence indicators to assess the formation of biodegradable dissolved organic carbon and bromate during ozonation. Water Res. 111, 154–162.
Luo, S., Wei, Z., Dionysiou, D.D., Spinney, R., Hu, W.-P., Chai, L., Yang, Z., Ye, T., Xiao, R., 2017. Mechanistic insight into reactivity of sulfate radical with aromatic contaminants through single-electron transfer pathway. Chem. Eng. J. 327, 1056–1065.
Lutze, H.V., Bircher, S., Rapp, I., Kerlin, N., Bakkour, R., Geisler, M., von Sonntag, C., Schmidt, T.C., 2015a. Degradation of chlorotriazine pesticides by sulfate radicals and the influence of organic matter. Environ. Sci. Technol. 49 (3), 1673–1680.
Lutze, H.V., Kerlin, N., Schmidt, T.C., 2015b. Sulfate radical-based water treatment in presence of chloride: formation of chlorate, inter-conversion of sulfate radicals into hydroxyl radicals and influence of bicarbonate. Water Res. 72, 349–360.
Madhavan, V., Levanon, H., Neta, P., 1978. Decarboxylation by SO_4^{-} radicals. Radiat. Res. 76 (1), 15–22.
Milne, C.J., Kinniburgh, D.G., Van Riemsdijk, W.H., Tipping, E., 2003. Generic NICA–Donnan model parameters for metal-ion binding by humic substances. Environ. Sci. Technol. 37 (5), 958–971.
Neta, P., Madhavan, V., Zemel, H., Fessenden, R.W., 1977. Rate constants and mechanism of reaction of sulfate radical anion with aromatic compounds. J. Am. Chem. Soc. 99 (1), 163–164.
Neta, P., Huie, R.E., Ross, A.B., 1988. Rate constants for reactions of inorganic radicals in aqueous solution. J. Phys. Chem. Ref. Data 17 (3), 1027–1284.
Nihemaiti, M., Miklos, D.B., Hübner, U., Linden, K.G., Drewes, J.E., Croué, J.-P., 2018. Removal of trace organic chemicals in wastewater effluent by UV/H_2O_2 and UV/PDS. Water Res. 145, 487–497.
Ramseier, M.K., Gunten, U.v., 2009. Mechanisms of phenol ozonation—kinetics of formation of primary and secondary reaction products. Ozone: Sci. Eng. 31 (3), 201–215.
Rosario-Ortiz, F.L., Wert, E.C., Snyder, S.A., 2010. Evaluation of UV/H_2O_2 treatment for the oxidation of pharmaceuticals in wastewater. Water Res. 44 (5), 1440–1448.
Sarathy, S., Mohseni, M., 2008. The fate of natural organic matter during UV/H_2O_2 advanced oxidation of drinking water. Can. J. Civ. Eng. 36 (1), 160–169.
Siegrist, R.L., Crimi, M., Simpkin, T.J., 2011. In Situ Chemical Oxidation for Groundwater Remediation. Springer Science & Business Media.
Tian, J., Wu, C., Yu, H., Gao, S., Li, G., Cui, F., Qu, F., 2018. Applying ultraviolet/persulfate (UV/PS) pre-oxidation for controlling ultrafiltration membrane fouling by natural organic matter (NOM) in surface water. Water Res. 132, 190–199.
Varanasi, L., Coscarelli, E., Khaksari, M., Mazzoleni, L.R., Minakata, D., 2018. Transformations of dissolved organic matter induced by UV photolysis, Hydroxyl radicals, chlorine radicals, and sulfate radicals in aqueous-phase UV-Based advanced oxidation processes. Water Res. 135, 22–30.
Wacławek, S., Lutze, H.V., Grübel, K., Padil, V.V.T., Černík, M., Dionysiou, D.D., 2017. Chemistry of persulfates in water and wastewater treatment: a review. Chem. Eng. J. 330, 44–62.
Wang, Y., Le Roux, J., Zhang, T., Croué, J.-P., 2014. formation of brominated disinfection byproducts from natural organic matter isolates and model compounds in a sulfate radical-based oxidation process. Environ. Sci. Technol. 48 (24), 14534–14542.
Wang, W.-L., Zhang, X., Wu, Q.-Y., Du, Y., Hu, H.-Y., 2017. Degradation of natural organic matter by UV/chlorine oxidation: molecular decomposition, formation of oxidation byproducts and cytotoxicity. Water Res. 124, 251–258.
Wenk, J., Aeschbacher, M., Salhi, E., Canonica, S., von Gunten, U., Sander, M., 2013. Chemical oxidation of dissolved organic matter by chlorine dioxide, chlorine, and ozone: effects on its optical and antioxidant properties. Environ. Sci. Technol. 47 (19), 11147–11156.
Westerhoff, P., Chao, P., Mash, H., 2004. Reactivity of natural organic matter with aqueous chlorine and bromine. Water Res. 38 (6), 1502–1513.
Westerhoff, P., Mezyk, S.P., Cooper, W.J., Minakata, D., 2007. Electron pulse radiolysis determination of hydroxyl radical rate constants with Suwannee River fulvic acid and other dissolved organic matter isolates. Environ. Sci. Technol. 41 (13), 4640–4646.
Xiao, R., Ye, T., Wei, Z., Luo, S., Yang, Z., Spinney, R., 2015. Quantitative structure–activity relationship (QSAR) for the oxidation of trace organic contaminants by sulfate radical. Environ. Sci. Technol. 49 (22), 13394–13402.
Xie, P., Ma, J., Liu, W., Zou, J., Yue, S., 2015. Impact of UV/persulfate pretreatment on the formation of disinfection byproducts during subsequent chlorination of natural organic matter. Chem. Eng. J. 269, 203–211.
Yang, Y., Lu, X., Jiang, J., Ma, J., Liu, G., Cao, Y., Liu, W., Li, J., Pang, S., Kong, X., Luo, C., 2017. Degradation of sulfamethoxazole by UV, UV/H_2O_2 and UV/persulfate (PDS): formation of oxidation products and effect of bicarbonate. Water Res. 118, 196–207.
Yang, Y., Cao, Y., Jiang, J., Lu, X., Ma, J., Pang, S., Li, J., Liu, Y., Zhou, Y., Guan, C., 2019. Comparative study on degradation of propranolol and formation of oxidation products by UV/H_2O_2 and UV/persulfate (PDS). Water Res. 149, 543–552.
Zhang, Z., Edwards, J.O., 1992. Chain lengths in the decomposition of peroxomonosulfate catalyzed by cobalt and vanadium. Rate law for catalysis by vanadium. Inorg. Chem. 31 (17), 3514–3517.
Zhang, H., Zhang, Y., Shi, Q., Ren, S., Yu, J., Ji, F., Luo, W., Yang, M., 2012. Characterization of low molecular weight dissolved natural organic matter along the treatment trait of a waterworks using Fourier transform ion cyclotron resonance mass spectrometry. Water Res. 46 (16), 5197–5204.
Zhang, T., Chen, Y., Leiknes, T., 2016. Oxidation of refractory benzothiazoles with PMS/CuFe2O4: kinetics and transformation intermediates. Environ. Sci. Technol. 50 (11), 5864–5873.
Zhou, Y., Jiang, J., Gao, Y., Ma, J., Pang, S.-Y., Li, J., Lu, X.-T., Yuan, L.-P., 2015. Activation of peroxymonosulfate by benzoquinone: a novel nonradical oxidation process. Environ. Sci. Technol. 49 (21), 12941–12950.
Zhou, L., Sleiman, M., Ferronato, C., Chovelon, J.-M., Richard, C., 2017. Reactivity of sulfate radicals with natural organic matters. Environ. Chem. Lett. 15 (4), 733–737.